LJMU Research Online

Godon, P, Sion, EM, Williams, RE, Darnley, MJ, Sokoloski, JL and Lawrence, SS

 The Accelerating Decline of the Mass Transfer Rate in the Recurrent Nova T Pyxidis

http://researchonline.ljmu.ac.uk/id/eprint/24757/

Article

For more information please contact researchonline@ljmu.ac.uk

The Accelerating Decline of the Mass Transfer Rate in the Recurrent Nova T Pyxidis[*]

Patrick Godon[1] , Edward M. Sion[1] , Robert E. Williams[2] , Matthew J. Darnley[3] , Jennifer L. Sokoloski[4] , and
Stephen S. Lawrence[5]

[1] Department of Physics and Planetary Science, Villanova University, Villanova, PA 19085, USA; patrick.godon@villanova.edu
[2] Space Telescope Science Institute, Baltimore, MD 21218, USA
[3] Astrophysics Research Institute, Liverpool John Moores University, IC2 Liverpool Science Park, Liverpool L3 5RF, UK
[4] Columbia Astrophysics Laboratory and Department of Physics, Columbia University, New York, NY 10027, USA
[5] Department of Physics and Astronomy, Hofstra University, Hamstead, NY 11549, USA

Abstract

The recurrent nova T Pyxidis (T Pyx) has erupted six times since 1890, with its last outburst in 2011, and the relatively short recurrence time between classical nova explosions indicates that T Pyx must have a massive white dwarf (WD) accreting at a high rate. It is believed that, since its outburst in 1890, the mass transfer rate in T Pyx was very large due to a feedback loop where the secondary is heated by the hot WD. The feedback loop has been slowly shutting off, reducing the mass transfer rate, and thereby explaining the magnitude decline of T Pyx from ∼13.8 (before 1890) to 15.7 just before the 2011 eruption. We present an analysis of the latest Hubble Space Telescope far-ultraviolet and optical spectra, obtained 12 yr after the 2011 outburst, showing that the mass transfer rate has been steadily declining and is now below its preoutburst level by about 40%: $\dot{M} \sim 1 - 3 \times 10^{-7} M_{\odot}\,\mathrm{yr}^{-1}$ for a WD mass of ∼1.0–1.4 $M_{\odot}$, an inclination of 50°–60°, reddening of $E(B-V) = 0.30 \pm 0.05$, and a Gaia Data Release 3 distance of 2860^{+816}_{-471} pc. This steady decrease in the mass transfer rate in the ∼decade after the 2011 outburst is in sharp contrast with the more constant preoutburst ultraviolet continuum flux level from archival International Ultraviolet Explorer spectra. The flux (i.e., $\dot{M}$) decline rate is 29 times faster now in the last ∼decade than observed since 1890 to ∼2010. The feedback loop shut off seems to be accelerating, at least in the decade following its 2011 outburst. In all eventualities, our analysis confirms that T Pyx is going through an unusually peculiar short-lived phase.

Unified Astronomy Thesaurus concepts: White dwarf stars (1799); Stellar accretion disks (1579); Cataclysmic variable stars (203); Recurrent novae (1366)

1. Introduction

Cataclysmic variables (CVs) are short-period interacting binaries where a white dwarf (WD) star accretes matter from its companion star (the donor) filling its Roche lobe. The transfer of material can be continue (as for UX UMa nova-like stars), sporadic (as for VY Scl nova-like stars and some dwarf nova systems), or almost periodic (as for many dwarf novae) and translates into a change in luminosity on timescales of days to months or even years (e.g., M. Hack et al. 1993; C. La Dous 1994). Over time (years to millennia), the accreting WDs in CVs accumulate a layer of hydrogen-rich material which, when the layer has reached a critical mass, provides enough temperature and pressure at its base to initiate a thermonuclear runaway (TNR): the classical nova explosion (or simply nova; E. Schatzman 1949; B. Paczyński 1965; S. Starrfield et al. 1972). The larger the WD mass and the higher the mass accretion rate onto it, the shorter the recurring time between such TNR nova explosions (e.g., O. Yaron et al. 2005; see also the remarkable recurrent nova (RN) M31N 2008-12a, with annual eruptions; M. H. Darnley et al. 2017). CVs that have suffered a classical nova explosion are called novae, and those

that have experienced more than one nova explosion are referred to as RNe (for a review on classical novae, see M. F. Bode & A. Evans 2008). While mass accumulates onto the WD during quiescence between recurring nova explosions, mass is also ejected during the nova explosions themselves, and the question whether the WD mass increases or decreases over its lifetime is still a matter of debate (Y. Hillman et al. 2020; S. Starrfield et al. 2020; Y. Hillman 2021). As a consequence, RNe are potential progenitors of Type Ia supernovae as their WD may grow in mass and reach the Chandrasekhar limit for a supernova explosion (J. Whelan & I. Iben 1973; see M. Livio & J. E. Pringle 2011 for a review). As such, accreting WDs in CVs are the site of some of the most violent eruptions in the Galaxy, exhibiting large luminosity changes on timescales of ∼days to millennia.

T Pyxidis (T Pyx) is a CV that has had six nova eruptions since 1890: in 1902, 1920, 1944, 1967, and with the last outburst in 2011 (B. E. Schaefer et al. 2013). Because of that, T Pyx is one of the most-studied RNe, it has also become one of the most enigmatic RNe, and certainly the most famous RN in the Milky Way. T Pyx is one of the three known short orbital period RNe (together with IM Nor and CI Aql), it is the only RN with a nova shell (H. W. Duerbeck & W. C. Seitter 1979), and its rise to outburst is characterized as slow (B. E. Schaefer et al. 2010). The expansion of the shell is believed to have originated from a normal classical nova eruption around the year 1866 (B. E. Schaefer et al. 2010).

Its relatively short (and increasing) recurrence time (12, 18, 24, 23, and 44 yr) indicates, on theoretical grounds (S. Starrfield et al. 1985), that its WD must be massive and accreting at a

Table 1
T Pyx System Parameters

| Parameter | P_{orb} | i | Π - Gaia | d | $E(B-V)$ | M_{wd} |
Units	(hr)	(deg)	(mas)	(pc)		$(M_\odot)$
Adopted Value	1.8295	50–60	0.34674 ± 0.0287	2860^{+816}_{-471}	0.30 ± 0.05	1.0, 1.2, 1.37

Note. Unless otherwise specified, these are the values of the system parameters we used in the present analysis of the 2023 HST spectra (see text for details).

high rate (possibly $\dot{M} \sim 1$–$2 \times 10^{-7} M_\odot$ yr^{-1}; O. Yaron et al. 2005). And indeed, optical and ultraviolet (UV) analyses (e.g., P. Selvelli et al. 2008; J. Patterson et al. 2017; P. Godon et al. 2018) have derived a mass transfer rate (disk luminosity) anywhere between 10^{-6} and 10^{-8} $M_\odot$ yr^{-1} (depending on the assumed WD mass, distance, reddening, and inclination). However, with an orbital period of 1.83 hr, the mass transfer rate (due to angular momentum loss by gravitational radiation) should be very low, of the order 2×10^{-11} $M_\odot$ yr^{-1}, as it is the case for CV systems with an orbital period below 2 hr (J. Patterson 1984). In order to explain the mass transfer/accretion[6] rate discrepancy of T Pyx and other novae, several theories have been advanced.

M. M. Shara et al. (1986) suggested that novae hibernate for millennia between eruptions to explain their (very low) space density in the solar neighborhood and justify the fact that old novae have low $\dot{M}$ while recent novae have a higher mass accretion. During a nova eruption, mass loss dominates, increasing the binary separation and Roche lobe radius. As a consequence, the secondary loses contact with the inflated Roche lobe and mass transfer basically stops after the eruption and after irradiation from the cooling WD becomes negligible. This explains the high $\dot{M}$ after the eruption and its decline thereafter, up to the point where hibernation starts ($\dot{M} < 10^{-12} M_\odot$ yr^{-1}), lasting thousands of years, during which the binary separation decreases slowly due to angular momentum loss from magnetic breaking (above the gap) or gravitational radiation (below the gap). M. M. Shara et al. (1986) suggested that in this manner most novae spend 90%–99% of their lives as a detached binary. In this scenario, the high mass transfer rate would have been sustained by the irradiation of the secondary by the WD, itself heated due to accretion (C. Knigge et al. 2000). Such a self-sustained feedback loop process would have been triggered during a classical nova eruption in 1866 (B. E. Schaefer et al. 2010), where the high mass accretion rate would occur with nuclear burning on the WD surface (self-sustained supersoft source). However, it has been shown (see B. E. Schaefer et al. 2013, Figure 1), that the B magnitude of T Pyx has been steadily decreasing from $B = 13.8$ before the 1890 eruption to $B = 15.7$ just before the 2011 eruption, indicating that the self-sustained feedback loop between the WD and secondary might be shutting off, in agreement with the hibernation theory.

It has also been proposed (C. Knigge et al. 2022) that the high mass transfer rate in T Pyx could be the result of the evolution of a triple star system, where the inner binary (WD + donor star) would become so eccentric that mass transfer is triggered at periastron, driving the secondary out of thermal equilibrium.

J. Patterson et al. (2017) showed that with a mass transfer rate of $\sim 10^{-7}$ $M_\odot$ yr^{-1} and a nova ejecta mass of 3×10^{-5} $M_\odot$ (6.7 times larger than the accreted mass between novae), the present series of nova eruptions are eroding the WD, and the secondary will evaporate in 10^5 yr, unless the RN eruptions are short-lived.

All these analyses agree that T Pyx must be going through a very unusual and short-lived phase in its life (according to J. Patterson et al. 2017, possibly its last phase).

In the current work, we present an analysis of the latest Hubble Space Telescope (HST) UV and optical spectra from 2023 March. The UV spectrum was obtained with the Cosmic Origin Spectrograph (COS), while the optical spectrum was obtained using the Space Telescope Imaging Spectrograph (STIS). This is the first combined optical (STIS) and far-ultraviolet (FUV) COS spectroscopic observation of T Pyx during the deep quiescent phase to model the accretion disk: the inner disk radiates mainly in the UV, while the outer disk radiates mainly in the optical. The results of our analysis indicate that the mass accretion rate is still decreasing compared to the HST data from 2015 to 2016 (P. Godon et al. 2018) and 2012 to 2013 (P. Godon et al. 2014), and it has now reached a level that is 40% below its preoutburst International Ultraviolet Explorer (IUE) value. Such a steady decrease in $\dot{M}$ is unexpected, since all the IUE spectra obtained through the 90s have the same flux level as the 1980 IUE spectrum and show no drop in flux (except for orbital variation). This could indicate that the decrease in the mass transfer rate started to accelerate after the 2011 outburst.

In Section 2 we discuss the system parameters that we adopted in the present work. In Section 3 we present the latest HST data together with the archival data for our analysis. The tools we used and the results obtained are presented in Section 4, follow by a discussion and summary in Section 5.

2. System Parameters

In our previous analysis of T Pyx (P. Godon et al. 2018) we analyzed HST COS UV spectra obtained in 2015 October and 2016 June and investigated the effect of the assumed WD mass (0.7 $M_\odot \leqslant M_{wd} \leqslant 1.35$ $M_\odot$), reddening ($0.25 \leqslant E(B-V) \leqslant 0.50$), distance ($2.8$ kpc $\leqslant d \leqslant 4.8$ kpc), and inclination ($20° \leqslant i \leqslant 60°$) on the results ($\dot{M}$). Therefore, we will not repeat this in the current work. Instead, and unless otherwise indicated, we assume here a large WD mass ($M_{wd} = 1.00$–1.37 $M_\odot$), a reddening of $E(B-V) = 0.30 \pm 0.05$, a Gaia Data Release 3 (DR3) parallax-derived distance of 2860^{+816}_{-471} pc, and an inclination $i = 50°$–$60°$. Below we justify our choice. The values of the system parameters we use for the analysis are listed in Table 1.

Taking the latest DR3 Gaia parallax to the system and following B. E. Schaefer (2018), we compute a distance of 2860^{+816}_{-471} pc, which is smaller than the distance originally

---

[6] Note that we are neglecting here any outflow from the disk and WD and use the term "mass transfer rate" when considering the disk (or the Roche lobe overflow of the secondary), and "mass accretion rate" when considering the accretion disk and WD, assuming that they are nearly equal; we use $\dot{M}$ for both. It is understood that the mass accretion rate might be slightly smaller than the mass transfer rate due to a possible outflow.

derived from light echoes (4.8 ± 0.5 pc; J. Sokoloski et al. 2013) and the distance we used in our previous spectral analysis based on the Data Release 2 Gaia parallax 3277^{+521}_{-395} pc; P. Godon et al. 2018).

Using recent data from the Multi Unit Spectroscopic Explorer from the European Southern Observatory in Chile, L. Izzo et al. (2024) characterize the morphology of the ejecta surrounding the system. They found that the expelled material consists of a ring of matter together with a bipolar outflow perpendicular to the ring. The inclination of the remnant along the line of sight is $i = 63°7$, and is expanding at a velocity of 472^{+77}_{-72} km s^{-1}. They put an upper limit to the bipolar outflow ejecta mass, $M_{\rm ej,b} < (3 \pm 1) \times 10^{-6} \, M_\odot$, which is lower than previous estimates. It is believed that the bipolar outflow originated from the 2011 outburst (since it was not observed before, and was first observed by HST in 2014). Consequently, we consider here an inclination $i \approx 50°–60°$ (as suggested by J. Patterson et al. 2017) to account for the large-amplitude ($\sim$20%) optical and UV modulations in the continuum flux level as a function of the orbital phase and to agree with the analysis of L. Izzo et al. (2024).

As to the WD mass, on the one hand, based on the short recurrence time of the T Pyx outbursts (of the order of 20 yr or so), theory predicts (e.g., S. Starrfield et al. 1985; R. F. Webbink et al. 1987; B. E. Schaefer et al. 2010) that the WD in T Pyx must be very massive (possibly near-Chandrasekhar: $1.37 \, M_\odot$; P. Selvelli et al. 2008) and accreting at a very large rate. On the other hand, X-ray observational evidence tends to point to a lower mass of the order of 1.00–$1.15 \, M_\odot$ (e.g., B. M. Tofflemire et al. 2013; L. Chomiuk et al. 2014, based on X-ray observations in the months/year following the 2011 outburst). Accordingly, in the current analysis we assume WD masses $M_{\rm wd} = 1.0, 1.2,$ and $1.37 \, M_\odot$, and we disregard the low WD mass ($0.7 \, M_\odot$) derived by H. Uthas et al. (2010), since it was retracted (C. Knigge 2019, private communication). This is in line with M. M. Shara et al. (2018) who showed that extensive simulations of nova eruptions combined together with observational databases of outburst characteristics of Galactic classical novae and RNe yield for T Pyx a WD mass of $1.23 \, M_\odot$ ($\pm 0.1 \, M_\odot$ or so) with a mass accretion rate of $6.3 \times 10^{-8} \, M_\odot$ yr^{-1} (but no error estimated given on $\dot{M}$) for the 44 yr interoutburst period between 1967 and 2011.

For the reddening we limit ourselves to the value we derived previously in P. Godon et al. (2018).

We must stress that the uncertainties in the values of the system parameters (WD mass, distance, inclination, extinction, chemical abundances, etc., which are used a input for the analysis) are relatively much larger than the errors in the analysis results that depend on them.

3. The Data

In this research we analyze the most recent HST UV–optical spectral data we obtained in 2023. For comparison and to complement the analysis we also present the HST UV data we obtained in 2018–2019, HST UV data from our previous analyses (2012, 2013, 2015, and 2016), IUE preoutburst data, and some never published HST optical data obtained in 2014. Since the IUE data and our previous HST UV data were already presented in P. Godon et al. (2018), we tabulate here only the data that were not presented elsewhere: COS UV data from 2018 October, 2019 February, and 2023 March; STIS optical data from 2023 March; and STIS optical data obtained

in 2014 (PI: A. Crotts), which were never published. All the data are listed in Table 2.

These observations were obtained with four different instrument configurations as follows.

1. The COS instrument (FUV MAMA, TIME-TAG mode) was set up with the PSA aperture, with the G130M grating with a central wavelength of 1055 Å, producing a spectrum starting at 925 Å all the way to 1200 Å, with a small gap near 1050 Å (and therefore covering all the series of the hydrogen Lyman transitions, except Lyα).

2. The COS instrument (FUV MAMA, TIME-TAG mode) was set up with the PSA aperture, with the G140L grating with a central wavelength of 1105 Å, producing a spectrum from 1100 Å to $\sim$2100 Å, covering the H Lyα absorption feature.

3. The STIS instrument (CCD, ACCUM mode) was set up with the G430L grating centered at 4300 Å, generating a spectrum from $\sim$3000 Å to $\sim$5700 Å.

4. The STIS instrument (CCD, ACCUM mode) was set up with the G750L grating centered at 7751 Å, generating a spectrum from $\sim$5250 Å to almost 10000 Å, thereby covering the optical and near-infrared (NIR) region.

The COS data were processed with CALCOS version 3.4.4 and the STIS data were processed with CALSTIS version 3.4.2. We used the x1d and sx1 files to extract the 1D spectra from each individual exposure, and used the x1dsum files to extract spectra from the coadded exposures (such as for the COS data obtained at four different positions of the detector).

3.1. The 2023 HST COS Far-ultraviolet and STIS Optical Data

The 2023 data consist of one of each instrument configuration above and were all obtained concurrently, the same day, 2023 March 24, between about midnight to 11:00—see Table 2. Namely the 2023 data cover the FUV, UV, optical, and NIR, and produce the only concurrent UV–optical–NIR spectra of T Pyx from $\sim$900 Å to $\sim$10000 Å (with a gap between 2000 Å and 3000 Å). These four concurrent UV–optical spectra are of special importance, since they are the only ones obtained concurrently after the 2011 outburst and during deep quiescence when all the emission is from the accretion disk. These four 2023 spectra are the focus of the present analysis and are modeled in Section 4 with an accretion disk. We present these four spectra in Figures 1, 2, 3, and 4, in order of increasing wavelength.

The short-wavelength COS (FUV) spectrum is displayed in Figure 1 on four panels, which is very noisy below 1090 Å (first/upper panel). All the absorption lines are from the interstellar medium (ISM), dominated mainly by molecular hydrogen (H_2), with some C I and Fe II lines. The identification of H_2 molecular lines by their band, upper vibrational level, and rotational transition can be found, e.g., in K. R. Sembach et al. (2001). The rather flat shape of the continuum flux level indicates that the emitting source is rather hot and is consistent with the inner part of the accretion disk.

The long-wavelength COS (UV) spectrum is displayed in Figure 2, also on four panels. Except for the N V doublet (which is blueshifted by $\sim$6 Å), all the absorption lines are from the ISM. Due to the relatively lower continuum flux level during deep quiescence, the signal-to-noise ratio is not high

Table 2
Observation Log

Instrument	Apertures	Filter Gratings	Central λ(Å)	Date (yyyy-mm-dd)	Time (hh:mm:ss)	Exp. Time (s)	Data ID	MODE	Project ID
STIS	52x0.1	G430L	4300	2023-03-24	08:18:47	1699	OEWH02010	ACCUM	17190
STIS	52x0.1	G750L	7751	2023-03-24	10:26:35	2340	OEWH02020	ACCUM	17190
COS	PSA	G140L	1105	2023-03-24	00:19:41	1912	LEWH01010	TIME-TAG	17190
COS	PSA	G130M	1055	2023-03-24	01:46:13	2405	LEWH01020	TIME-TAG	17190
COS	PSA	G130M	1055	2019-02-01	12:58:11	1836	LDG002010	TIME-TAG	15184
COS	PSA	G140L	1105	2018-10-04	00:30:11	1876	LDG001010	TIME-TAG	15184
STIS	52x2	G430L	4300	2014-07-21	02:29:59	378	OCIQ02010	ACCUM	13796
					02:38:11	378	OCIQ02020	ACCUM	13796
					02:46:23	378	OCIQ02030	ACCUM	13796
					02:54:35	378	OCIQ02040	ACCUM	13796
					03:51:04	558	OCIQ02050	ACCUM	13796
					04:04:42	558	OCIQ02060	ACCUM	13796
					04:15:54	558	OCIQ02070	ACCUM	13796
					04:27:06	558	OCIQ02080	ACCUM	13796
					05:26:37	552	OCIQ02090	ACCUM	13796
					05:40:35	552	OCIQ020A0	ACCUM	13796
					05:51:41	552	OCIQ020B0	ACCUM	13796
					06:02:47	552	OCIQ020C0	ACCUM	13796
					07:08:57	544	OCIQ020D0	ACCUM	13796
					07:19:55	544	OCIQ020E0	ACCUM	13796
					07:30:53	544	OCIQ020F0	ACCUM	13796
					08:40:09	544	OCIQ020G0	ACCUM	13796
STIS	52x2	G750L	7751	2014-07-23	21:23:16	373	OCIQ03010	ACCUM	13796
					21:31:24	373	OCIQ03020	ACCUM	13796
					21:39:32	373	OCIQ03030	ACCUM	13796
					21:47:40	373	OCIQ03040	ACCUM	13796
					22:44:01	558	OCIQ03050	ACCUM	13796
					22:57:39	558	OCIQ03060	ACCUM	13796
					23:08:51	558	OCIQ03070	ACCUM	13796
					23:20:03	558	OCIQ03080	ACCUM	13796
				2014-07-24	00:19:33	552	OCIQ03090	ACCUM	13796
					00:33:31	552	OCIQ030A0	ACCUM	13796
					00:44:37	552	OCIQ030B0	ACCUM	13796
					00:55:43	552	OCIQ030C0	ACCUM	13796
					01:55:53	543	OCIQ030D0	ACCUM	13796
					02:06:51	543	OCIQ030E0	ACCUM	13796
					02:17:49	543	OCIQ030F0	ACCUM	13796
					02:28:47	543	OCIQ030G0	ACCUM	13796

Note. The time (hh:mm:ss) is the start time for each exposure. All the data presented were obtained from the Mikulski Archive for Space Telescope at the Space Telescope Science Institute, Baltimore, MD, USA. The specific spectral data listed above can be accessed via 10.17909/2d6h-qy95. COS data were processed through the pipelines with CALCOS version 3.4.4. STIS data were processed through the pipelines with CALSTIS version 3.4.2.

enough to detect all the ISM lines which were observed in the early phase following the outburst by A. De Gennaro et al. (2014).

Each COS spectrum is generated from the sum of four subexposures, each obtained on a different location on the detector. We checked the four subexposures from each of the two 2023 COS spectra and did not find, within the amplitude of the noise/error spectrum, any variation in the width, depth, and wavelength of the absorption lines that could reveal orbital modulation, even for the N V doublet. However, this is likely an indication that the subexposures are too noisy to extract any significant information. The rest wavelength of the N V doublet lines are 1238.821 Å and 1242.804 Å (A. Kramida et al. 2023), and to within ± 0.1 Å the observed wavelengths in the four subexposures are 1232.9 Å and 1237.0 Å, 1233.3 Å and 1237.1 Å, 1233.1 Å and 1237.0 Å, and 1233.0 Å and 1237.1 Å. This gives an average blueshift of $\sim 5.7 \pm 0.2$ Å, which at 1240 Å corresponds to a velocity of 1384 ± 49 km s^{-1}.

The STIS optical–NIR spectra are presented in Figures 3 and 4. Contrary to the previous optical spectra, these two spectra are not dominated by nebular emission, they exhibit absorption and emission lines from hydrogen and helium, and we tentatively identify some weak emission lines from C III (4650 Å) and [Fe VII] (5168 Å).

3.2. Earlier Archival Ultraviolet and Optical Data

The existing preoutburst UV archival data of T Pyx consist of more than 50 IUE short-wavelength prime + long-wavelength prime spectra from 1980 (~ 13 yr after the 1966 December–1967 January outburst) through the 90s and one Galaxy Evolution Explorer (GALEX; FUV + near-ultraviolet (NUV)) spectrum taken at the end of 2005. The preoutburst data reveal a UV continuum flux level remarkably constant, except for an orbital phase modulation.

The HST COS and STIS UV spectra, all obtained postoutburst, follow the decline of the system into its quiescent
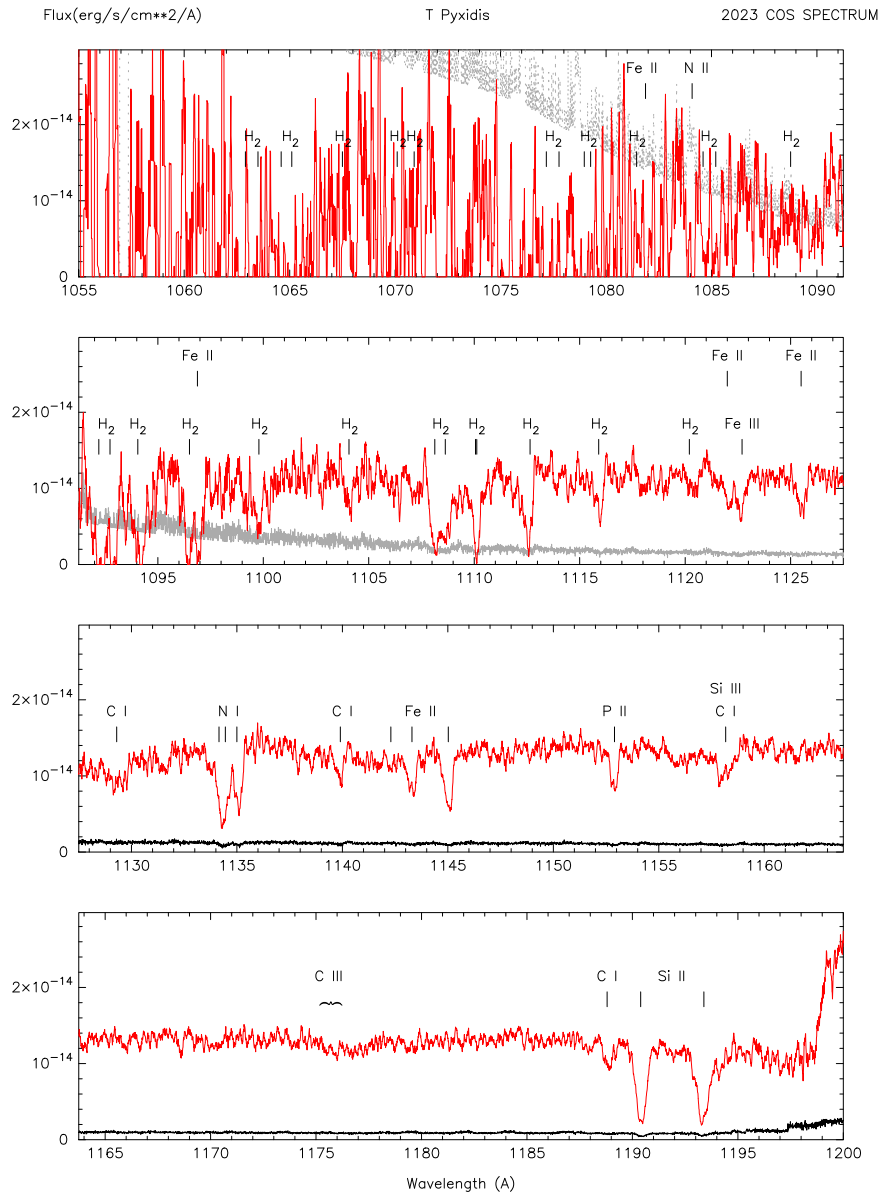
Figure 1. The 2023 HST COS G130M (1055 Å) spectrum of T Pyx with line identifications. The spectrum is shown in red; for convenience and clarity the error spectrum is shown in dashed gray in the upper/first panel, gray in the second panel, and black in the two lower panels. The spectrum has not been dereddened.

state, starting 2011 May. By 2012 December, the strong broad emission lines had disappeared and the UV continuum flux level had reached its preoutburst (IUE) level, after which the UV flux continued to decrease, but more slowly (see P. Godon et al. 2018, for a review).

We expected the UV decline would have reached a plateau by 2023, mimicking the postoutburst IUE data. However, since 2018 October the UV flux has further dropped by ∼20% and is now about 40% below its IUE preoutburst level—see Figure 5. Even the C IV (1550 Å) and He II (1640 Å) emission lines, which were prominent in the IUE preoutburst and HST postoutburst spectra, are now much reduced: the intensity of the C IV line in 2023 is ∼one-sixth of what it was in 2018, and that of the He II line is ∼one-third.

Note that the COS G130M 1055 Å spectra (Figure 5(a)) are extremely noisy below ∼1090 Å (as seen already in Figure 1). The 1150–1200 Å region of the 2023 COS G130M (1055 Å, red spectrum in Figure 5(a)) does not match the 2023 COS

G140L 1105 Å spectra (also red in Figure 5(b)). A similar discrepancy in fluxes was apparent in the 2015 October COS data of T Pyx (P. Godon et al. 2018) between the two configurations (G140L/1105 Å versus G130M/1055 Å), and, while some of the discrepancy could be attributed to orbital modulation, it is mainly due to calibration errors (edges of the detectors). The two Si II lines (1190.4 and 1193.3 Å) are clearly seen in the G130M (1055 Å) spectra (and even in the IUE spectrum; right edge of panel (a) of Figure 5) but they are absent in the G140M (1105 Å) spectra (blue and red spectra; left edge of panel (b) in Figure 5).

As T Pyx erupted in 2011, it became the target of several observing campaigns and many optical spectra were obtained with HST/STIS. The latest HST optical spectra of T Pyx collected before our current HST 2023 observation are from 2014 July: OCIQ020 (STIS G430L) and OCIQ030 (STIS G750L), made of 16 exposures each (see Table 2). All the optical STIS spectra following the outburst and through 2014
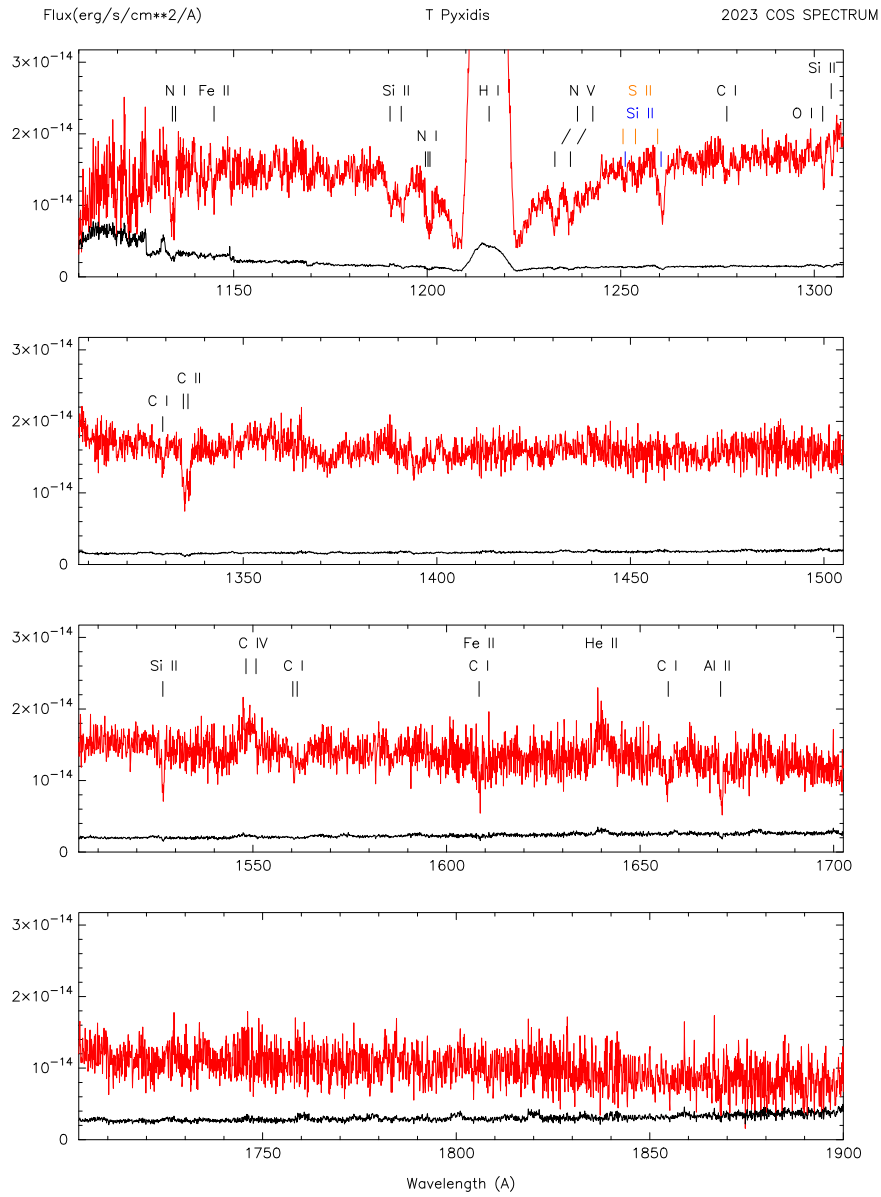
Figure 2. The 2023 HST COS G140L (1105 Å) spectrum of T Pyx with line identifications. The spectrum is shown in red, and the error spectrum is shown in black. The S I and Si II lines near 1250–1260 Å are shown in color so that they can be identified separately. Note the strongly blueshifted N V (1240 Å) doublet. The spectrum has not been dereddened.

July reveal the presence of nebular emission lines. We extracted the 32 1D spectra from the 2014 July STIS data (as listed in Table 2) and coadded the 16 exposures each for the OCIQ020 and OCIQ030 sets by weighting them by exposure time. We then combined the OCIQ020 and OCIQ030 spectra together. A comparison with the 2014 optical STIS spectra (Figure 6) reveals that the optical continuum flux level (near $\sim$4500 Å) has now dropped by $\sim$38% and the nebular emission lines have almost all completely disappeared. In the very long-wavelength range (near $\sim$8000 Å), corresponding to the NIR, the continuum flux level has dropped by $\sim$35%. Note that the 2014 and 2023 spectra displayed in Figure 6 were generated by coadding the individual exposures weighted by the exposure time for each of the COS configurations G430 and G750L. Since the G430 and G750L spectra cover less than the binary orbital period, their continuum flux level did not match perfectly. This is most apparent in the 2023 spectra, which have shorter exposure times ($\sim$2000 s) than the 2014 spectra

(totaling more than 8000 s, but covering only 80% of the binary orbital period due to the timing of the exposures). For the 2014 spectrum, the G750L segment has to be scaled down by $\sim$1% to match the G140M segment; for the 2023 spectrum, the G750 segment has to be scaled up by 7% to match the G140M segment.

4. Analysis

4.1. Variability

It has been well documented (B. E. Schaefer et al. 2013) that the B-band magnitude of T Pyx has been steadily decreasing from $B = 13.8$ in 1890 to $B = 15.7$ just before the 2011 eruption. And in recent years, as T Pyx returned to quiescence following the 2011 outburst, it has gradually become fainter from 15.8 to 16.1 (E. Waagen et al. 2023, private communication). In order to check the behavior of T Pyx in the UV, we generated a UV light curve of the system (P. Godon et al. 2018) using archival UV
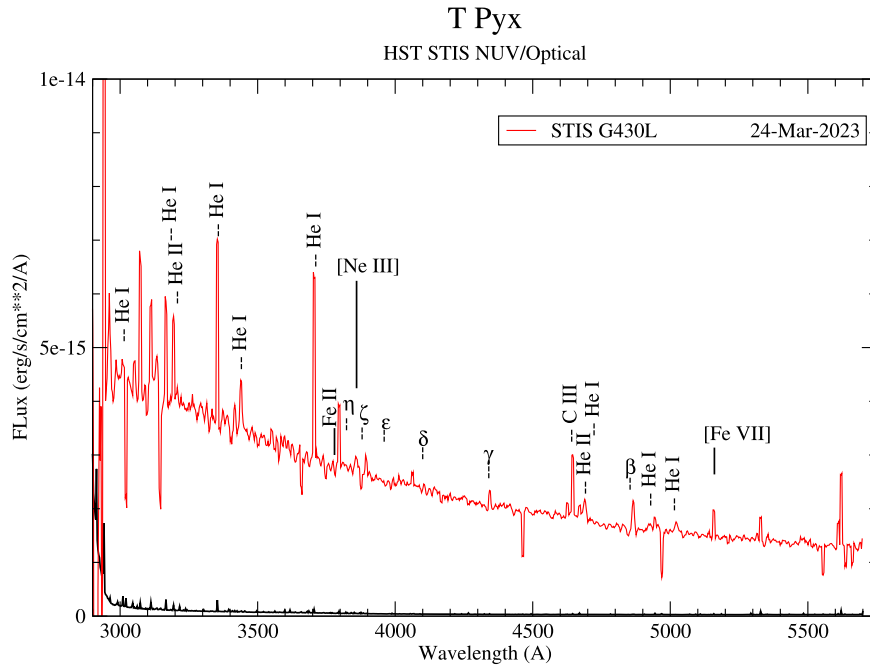
Figure 3. The 2023 HST STIS G430L (4300 Å) spectrum (in red) with line identifications; the error spectrum is shown in black. This spectrum has not been corrected for extinction.
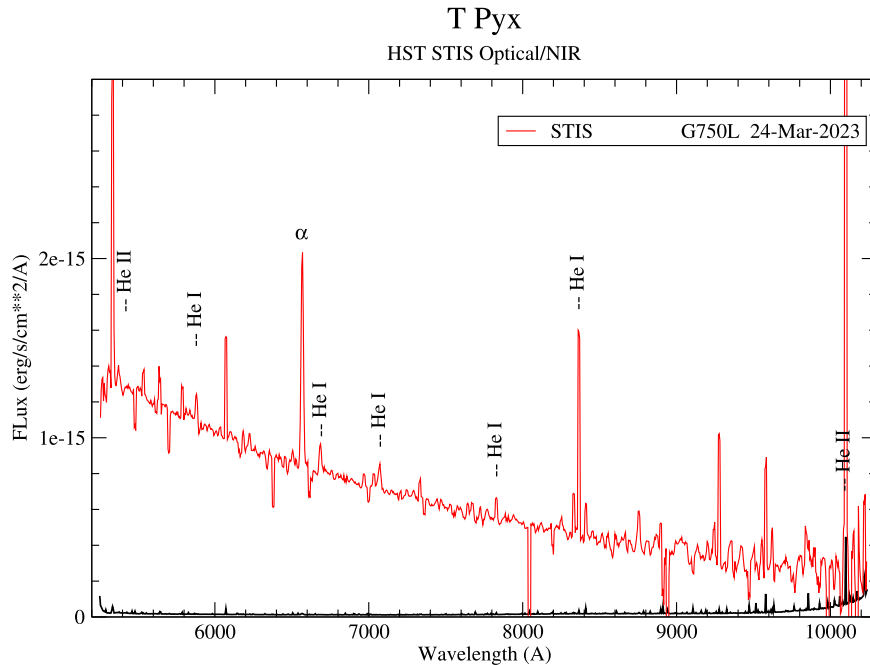

Figure 4. The 2023 HST STIS G750L (7751 Å) spectrum (in red) with line identifications (the error spectrum is shown in black). The spectrum exhibits mostly hydrogen and helium emission lines. This spectrum has not been corrected for extinction.

spectra from the IUE (from 1980 to 1996), GALEX (one spectrum obtained in 2005; see B. E. Schaefer et al. 2013), and HST STIS and COS UV spectra (following the 2011 outburst). We display in Figure 7 an updated UV light curve using the latest HST spectra (from 2023 and 2018). All the data points were obtained by integrating the UV spectral flux between 1400 Å and 1700 Å (excluding emission and absorption lines). The IUE do not reveal a decrease in the continuum flux level between 1980 and 1996, and clearly show a modulation Δ of up to 18% (i.e., $\pm9\%$) in the UV continuum flux level. Unfortunately, the IUE single exposures had all a duration of

~1 to ~2 times the binary orbital period, and a phase-resolved UV light curve could not be generated. However, we attribute this modulation to the orbital motion of the binary. Since the UV light curve shown in the figure results from an integration over a large spectral range, the flux error is much reduced and completely negligible in comparison to the uncertainty due to the orbital modulation. The HST data points also reveal orbital modulation but to a lesser extent since not every orbital phase was covered. Following the 2018 HST observation, we expected the UV flux to reach a plateau but the 2023 data point shows a further drop of 20% compared to the 2018 data. While we
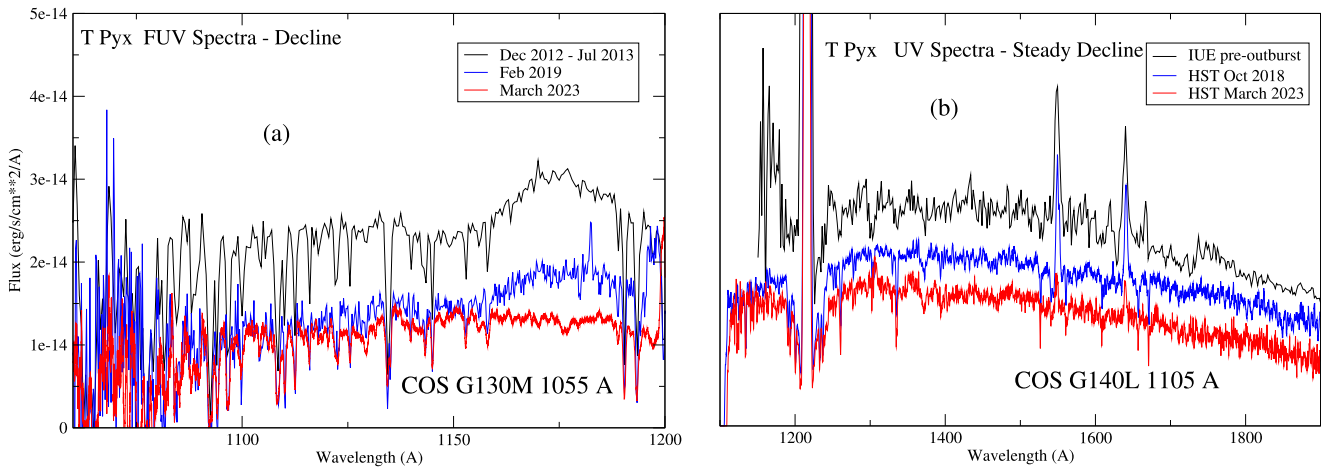
Figure 5. UV spectra of T Pyx showing a steady decline in the continuum flux level. In the short-wavelength region (FUV, panel (a)), the flux drop since 2018–2019 is not as large as in the longer wavelength region (mid-ultraviolet, panel (b)). In 2012–2013, the UV flux had reached its preoutburst level. In the region where the spectra overlap (~1150–1200 Å), the short-wavelength spectra (a) do not match the long-wavelength spectra (b) as they systematically appear to have a higher flux. The spectra are presented here before dereddening.
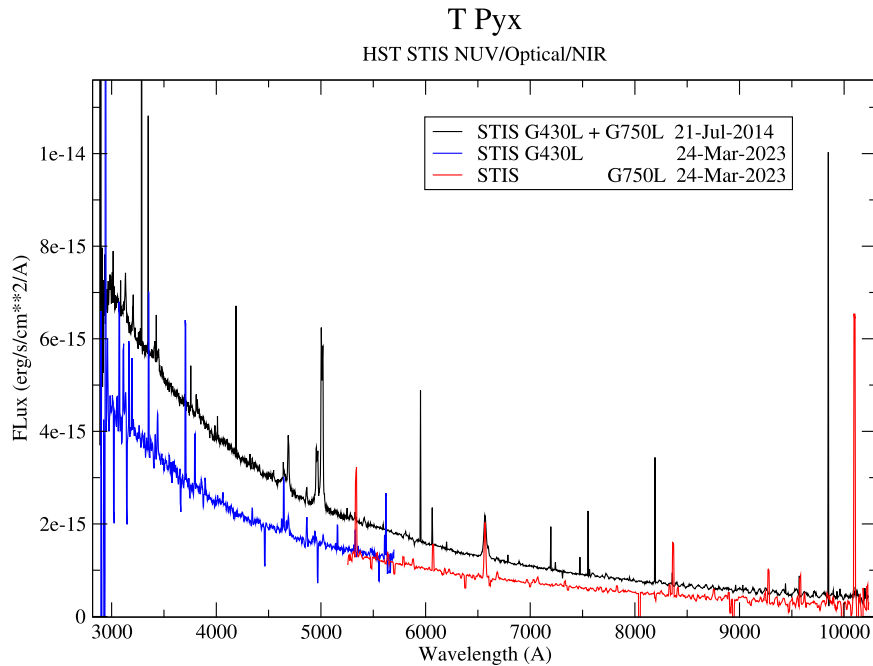
Figure 6. Comparison of the HST optical–NIR spectrum from 2023 (in blue and red) to the same spectrum obtained almost a decade earlier in 2014. The spectra have not been corrected for extinction.

cannot rule out that this could be due, in part, to orbital modulation, the UV light curve after the 2011 outburst definitely exhibits a trend consistent with a steady decline in sharp contrast with the preoutburst light curve.

As for most novae and RNe, many more HST observations were carried out during outburst and decline from outburst than during deep quiescence, and except for our current 2023 STIS optical spectrum, all the HST optical spectra were obtained between 2011 and 2014, while the system still showed nebular emission. Among these HST optical spectra we selected the STIS data sets OCIQ020 (G430L) and OCIQ030 (G750L), each with 16 exposures (see Table 2) from 2014 July; the emission lines of forbidden transitions forming in the nebular material are still present (see Figure 6). These two data sets were obtained only 2 days apart and while they cover different spectral wavelength regions, they do overlap between 5245 Å

and 5690 Å. We therefore integrated the flux of the 32 exposures between 5285 Å and 5655 Å (excluding emission lines), to compute the average continuum flux level in that wavelength region, which corresponds to the chartreuse color. In Figure 8 we present the chartreuse light curve folded at the orbital phase, which clearly reveals the orbital modulation of the continuum flux level with an amplitude of ±8%, similar to the UV data. The flux is minimum near phase 0.9, where the L1 stream is hitting the rim of the disk and indicates that the disk edge might be swollen and partially occulting the disk (self-occulting; see J. Patterson et al. 1998). The orbital phase values were computed using the postoutburst ephemerides provided by J. Patterson et al. (2017, Equation (2)), which take into account the period change of the system, and taking the midvalue of the observation times of each exposure listed in Table 2 (namely we added half the exposure time to the starting
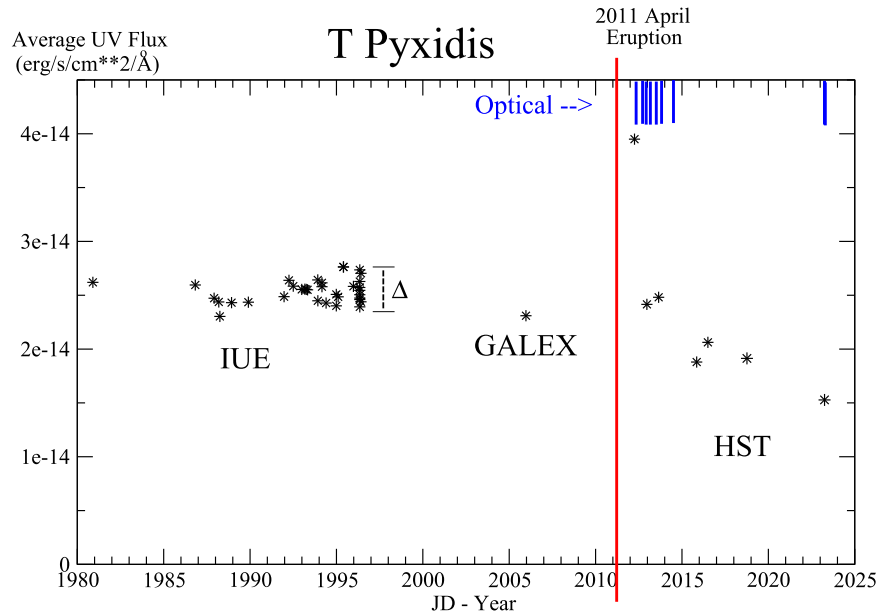
Figure 7. The average UV continuum flux level of T Pyx (black stars) over the spectral range [1400–1700] Å as a function of time (the data have not been corrected for extinction). The red vertical line represents the 2011 April outburst of the system. HST STIS optical spectra were also collected after the outburst and their timing is indicated using vertical blue lines at the top. This graph is an update of the one presented in P. Godon et al. (2018) and shows that the UV continuum flux level continues to drop well below its preoutburst level.
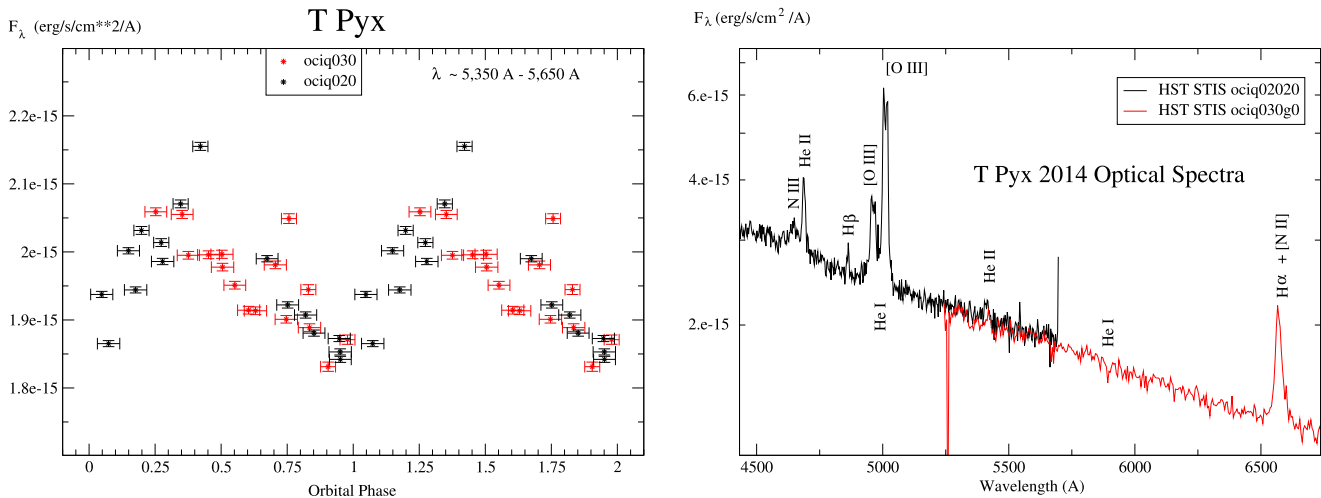
Figure 8. Left: the chartreuse light curve of T Pyx folded at the orbital phase revealing an orbital modulation. The chartreuse light-curve data were obtained from HST STIS archival data OCIQ020 (black dots) and OCIQ030 (red dots) integrated over the spectral wavelength range $\lambda \sim 5285$–5655 Å , where the grating G430L (centered at 4300 Å, for OCIQ020) overlaps with the grating G750L (centered at 7751 Å, for OCIQ030). The data sets OCIQ020 and OCIQ030 have 16 exposures each (see Table 2). Right: the overlap region of the two STIS data sets (OCIQ020 with G340L) and (OCIQ030 with G750L) is shown. For clarity, only one exposure for each STIS setting is shown here: OCIQ02020 in black and OCIQ030G0 in red. The flux (vertical) axis is displayed on a log scale. The data presented in this figure were not corrected for extinction.

time). The flux error on the integrated wavelength region is of the order of 5×10^{-18} erg s^{-1} cm^{-2} Å^{-1}, and the error on the orbital phase is taken as (half) the exposure time as listed in Table 2 for each exposure (namely 387/2 s for the first four exposures, 558/2 s for the next four, etc.).

4.2. The Spectral Slope

In P. Godon et al. (2018), we used archival optical and NUV (IUE and GALEX) spectra to supplement our HST FUV postoutburst spectra in our accretion disk modeling and found that the slope of the continuum flux level is flatter in the optical than in the UV. However, these preoutburst archival optical

and NUV data were not obtained concurrently with the same telescope, and the optical data were obtained from ground-based telescopes and digitally extracted from graphs. Therefore, we decided to carry out a new assessment of the slope of the spectrum using an updated and improved dereddening law and using UV and optical data obtained the same day with HST: the 2023 HST STIS and COS spectra. In the FUV, instead of using the extinction law of E. L. Fitzpatrick & D. Massa (2007; as we did in P. Godon et al. 2018), we used the standard curve of B. D. Savage & J. S. Mathis (1979), which gives a smaller correction in the FUV (and therefore a shallower slope in the FUV). This is in line with the analysis of T Pyx by P. Selvelli & R. Gilmozzi (2013), based on the work
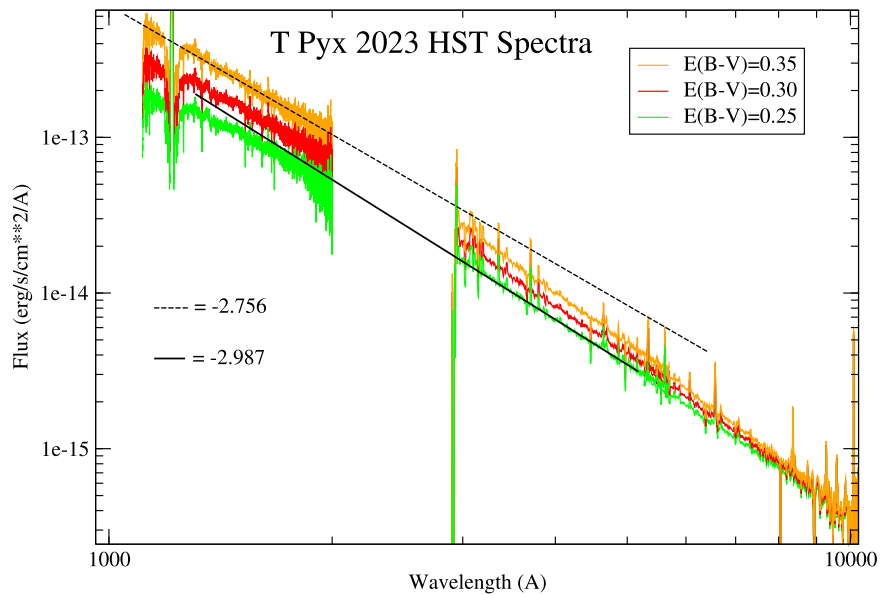
Figure 9. The HST UV–optical spectrum of T Pyx dereddened by $E(B-V) = 0.25$ (green), 0.30 (red), and 0.35 (orange), on a log–log scale. The slope of the continuum flux level is steeper in the optical than in the UV. Even for the larger dereddening, the slope of the continuum flux level in the UV (-2.76, dashed black line) is not as steep as the slope of continuum flux level in the optical, which has the shallowest slope of -2.99 (solid black line) for the smallest value of the dereddening considered here.

of T. P. Sasseen et al. (2002) who showed that in the FUV the observed extinction curve is consistent with an extrapolation of the standard extinction curve of Savage & Mathis (1979; further details and discussion on our choice of the extinction curve were given in P. Godon et al. 2020). In Figure 9 we display the combined 2023 (UV + optical + NIR) spectrum of T Pyx dereddened assuming $E(B-V) = 0.25$, 0.30, and 0.35 (the values we adopted) on a log–log scale of the flux F_λ (in units of erg s^{-1} cm^{-2} Å^{-1}) versus wavelength λ (in units of Å). The steepest (continuum) spectral slope in the UV (at wavelengths longer than the Lyα region, $\lambda > 1300$ Å) is obtained for a dereddening of $E(B-V) = 0.35$ and has value $\alpha = -2.76$, while the flattest optical ($\lambda \sim 3000$–6000 Å) slope is obtained for a dereddening of $E(B-V) = 0.25$ and gives a slope $\alpha = -2.99$, larger than the UV. At longer wavelength (NIR, $\lambda \sim 7000$–10000 Å) the slope steepens even more (< -3). Namely, we find that the spectral slope steepens with increasing wavelength, thereby confirming the findings of R. Gillmozzi & P. Selvelli (2007). This finding is valid for the values of $E(B-V)$ we (and R. Gillmozzi & P. Selvelli 2007) use when dereddening the spectra for the analysis of the T Pyx optical and UV data. While we found that both the UV and optical continuum flux levels vary by about the same amplitude as a function of the orbital phase, their slope did not reveal orbital modulation.

4.3. Accretion Disk Modeling and Spectral Analysis

The spectral analysis procedure we follow is extensively described in P. Godon et al. (2020) and only a short overview is given here. We use the suite of FORTRAN codes TLUSTY & SYSNPEC (I. Hubeny & T. Lanz 2017a, 2017b, 2017c) to generate accretion disk spectra for a given WD mass $M_{\rm wd}$, mass transfer rate $\dot{M}$, inclination i, and inner and outer disk radii ($r_{\rm in}$ and $r_{\rm out}$, respectively). The accretion disk is based on the standard disk model (N. I. Shakura & R. A. Sunyaev 1973; J. E. Pringle 1981), which is assumed to be optically thick and have solar composition. We generate a grid of disk spectra for

$M_{\rm wd} = 1.0$, 1.2, and 1.37 $M_\odot$, $r_{\rm in} = R_{\rm wd}$, 10^{-8} $M_\odot$ yr^{-1} $\leqslant \dot{M} \leqslant 10^{-6} M_\odot$ yr^{-1} (increasing or decreasing $\dot{M}$ in steps of $\sim 50\%$), and for $i = 50°$ and 60°. These theoretical spectra extend from 900 Å to 7500 Å.

We first assume a WD mass of 1.37 $M_\odot$, and it is understood that accretion disk model fits with a lower WD mass (see further down) will result in a larger mass accretion rate. With a secondary mass of 0.13 $M_\odot$ and an orbital period of 1.8295 hr, we obtain a binary separation of 585,592 km. For such a mass ratio ($\log(q) \approx -1.0$), the outer radius of the disk is expected to be tidally truncated at $r_d \approx 0.5$ a (Figure 3 in J. Goodman 1993), where a is the binary separation, while the Roche lobe radius of the WD is about 0.6 a. We note that for a mass ratio close to 1 the tidally truncated disk radius is close to 0.3 a (B. Paczyński 1977), while for a vanishingly small mass ratio it is close to 0.6 a (J. Goodman 1993). We compute disk models assuming an outer disk radius of 180,000 km (90 $R_{\rm wd}$) and 360,000 km (180 $R_{\rm wd}$), corresponding to about ~ 0.3 a and ~ 0.6 a, respectively (where we have assumed a 2000 km radius for T Pyx's WD). As we lower the WD mass to 1.0 $M_\odot$ we obtain a binary separation much closer to 5×10^5 km and vary the outer disk radius accordingly.

We first carry out accretion disk spectral fits assuming $M_{\rm wd} = 1.37$ $M_\odot$, and for the following values of the parameters: $i = 50°$ and 60°, outer disk radius $r_{\rm out} = 0.3$ a and 0.6 a, $E(B-V) = 0.25$, 30, and 35, and a Gaia distance of 2389 pc, 2860 pc, and 3676 pc (see Table 1 for the system parameters). For each set of (i, $r_{\rm out}$, $E(B-V)$, d) the spectral fits yields a unique value of the mass accretion rate $\dot{M}$.

In Figure 10 we display two of the accretion disk spectral fits we ran assuming an inclination of 50°, extinction $E(B-V) = 0.30$, and a Gaia distance of 2860 pc. In one model the disk was truncated at 0.6 a and in the second model it was truncated at 0.3 a. The resulting mass accretion rate is $\dot{M} = 1.07 \times 10^{-7} M_\odot$ yr^{-1} for the larger disk, versus 1.28×10^{-7} $M_\odot$ yr^{-1} for the smaller disk. Since most of the flux is emitted in the UV range, we mainly fit the UV region,
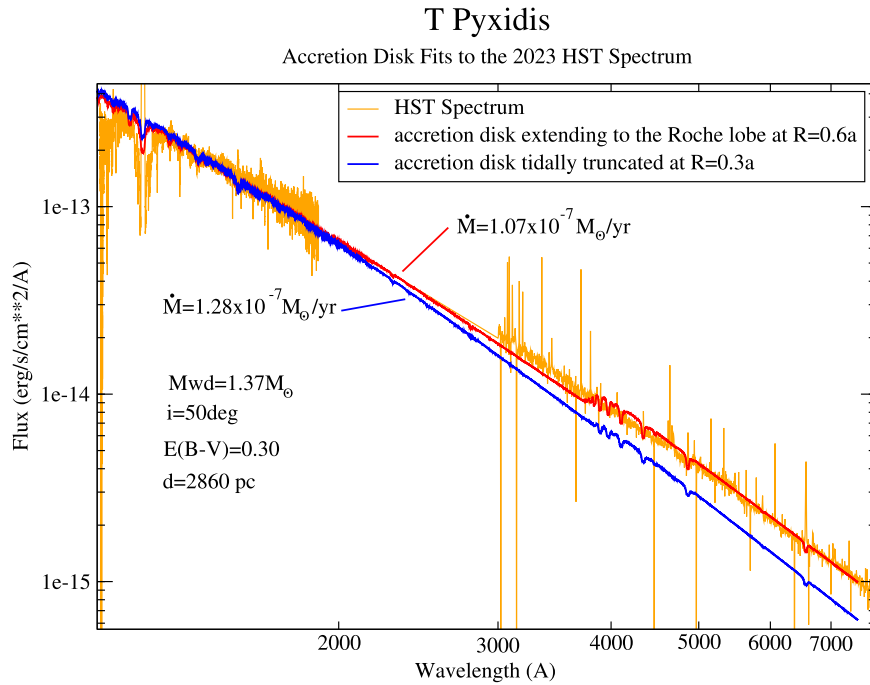
T Pyxidis
Accretion Disk Fits to the 2023 HST Spectrum

Figure 10. Accretion disk fits to the dereddened HST spectrum of T Pyx for a WD mass $M_{wd} = 1.37\ M_\odot$, inclination $i = 50°$, and a Gaia distance of 2860 pc. The results are presented on a log–log scale of the flux vs. wavelength. Assuming $E(B - V) = 0.30$, the HST spectrum (orange line) is fitted for a mass transfer rate $\dot{M} = 1.07 \times 10^{-7} M_\odot\ yr^{-1}$ when the disk extends to 0.6 a (red line). Assuming a disk truncated at $R = 0.3\ a$ (blue line) increases $\dot{M}$ to $1.28 \times 10^{-7}\ M_\odot\ yr^{-1}$ and produces a stepper slope.

and it appears immediately that the smaller disk does not fit the optical as it is too blue. On the other hand, the larger disk displays a small Balmer jump, which is not seen in the observed spectrum (we will expand on this issue in the next section).

While we are aware that it is likely that the disk radius is about 0.5 a, we ran models for both the 0.3 a and 0.6 a values. For all the values of the parameters considered here (and including their uncertainty), the results can be summarized as follows. We obtain a mass accretion rate of

$$\dot{M} = 1.38^{+1.17}_{-0.87} \times 10^{-7} M_\odot\ yr^{-1}$$

for

$$i = 55° \pm 5°, \quad \frac{r_{out}}{a} = 0.45 \pm 0.15,$$

$$E(B - V) = 0.30 \pm 0.05, \quad \text{and } d = 2860^{+816}_{-471}\ \text{pc},$$

assuming a near-Chandrasekhar WD mass of 1.37 $M_\odot$. The error in $\dot{M}$ is due mainly to the uncertainty in the distance and reddening, while the uncertainty in the value of the outer disk radius contributes less than 10% to the (relative) error in $\dot{M}$.

Next we assume a WD mass $M_{wd} = 1.2\ M_\odot$ and $M_{wd} = 1.0\ M_\odot$, and obtain similar results with a larger mass accretion rate

$$\dot{M} = 2.16^{+1.81}_{-1.36} \times 10^{-7} M_\odot\ yr^{-1}, \quad \text{and}$$

$$\dot{M} = 2.94^{+2.46}_{-1.85} \times 10^{-7} M_\odot\ yr^{-1},$$

for $M_{wd} = 1.2\ M_\odot$ and $M_{wd} = 1.0\ M_\odot$, respectively.

5. Discussion and Conclusion

The present UV–optical analysis shows that the mass accretion in T Pyx has been steadily decreasing, and is now of the order of $10^{-7}\ M_\odot\ yr^{-1}$ (based on the assumed system

parameters), about 40% lower than its preoutburst value assessed from archival IUE spectra. The decreased activity of the system is further supported by the weakened C IV (1550 Å) and He II (1640 Å) emission lines (in the COS G140L spectrum from 2023 March), which were prominent in the IUE preoutburst and HST postoutburst spectra. The mass accretion rate, however, cannot be determined accurately since the reddening, distance, and WD mass have not been themselves assessed with a high accuracy. The WD mass is assumed to be large ($\sim1\ M_\odot$ or even near-Chandrasekhar) on theoretical grounds (as explained in Section 1); the Gaia parallax has a relatively large error; and while we assume $E(B - V) = 0.30 \pm 0.05$, some authors have derived an extinction as large as $E(B - V) = 0.5 \pm 0.1$ (S. N. Shore et al. 2011). In our previous work we showed how the uncertainties in the system parameters (M_{wd}, $E(B - V)$, d, and i) affect the derived mass accretion rate by an order of magnitude: $\dot{M} \sim 10^{-7\pm1} M_\odot\ yr^{-1}$ (Figure 10 in P. Godon et al. 2018).

Another source of uncertainty is the chemical composition of the accretion disk. We assume solar abundances for the accretion disk, but the donor/secondary could have nonsolar abundances affecting the shape and slope of the disk spectrum (if highly suprasolar/hydrogen deficient). Here too the problem is that the state of the secondary star in T Pyx is unknown. Absorption lines of metals (i.e., $Z > 2$) for different temperatures in the disk cannot be detected due to the combined action of Keplerian broadening and superposition. As a consequence, it is the hydrogen content (and more precisely the [H/He] ratio) that dictates the general shape of the spectrum (P. Godon & E. M. Sion 2023), and only for small values of [H/He] (as observed for the secondary of QZ Ser with a 90% hydrogen deficit; T. E. Harrison 2018) is the shape of the spectrum noticeably affected. Hence, our solar composition results are valid as long as the actual metallicity of the accretion disk (and

therefore secondary donor star) does not depart too much from solar. This is a sound assumption, since even evolved-donor CV systems, with high N and low C abundances, are not all strongly hydrogen deficient (unlike QZ Ser, AE Aqr, DX And, and EY Cyt; J. R. Thorstensen et al. 2002; T. E. Harrison 2018). This is fortunate, since generating accretion disk models from scratch as a function of chemical abundances is prohibitively CPU expensive (as we already vary the disk input parameters such M_{wd}, $\dot{M}$, i, and the disk radius) and the version of TLUSTY we are using is not well suited to generating helium-dominated spectra.

In comparison to the above uncertainties in the system parameters, the systematic error in the modeling of the disk is rather negligible. Whether we chose a disk radius of 0.3 a or 0.6 a did not affect the results quantitatively as much as it did qualitatively. For a mass transfer rate of $\sim 10^{-7}$ $M_{\odot}$ yr^{-1}, the temperature in the disk at $r = 0.3$ a is 25,000 K and drops to 15,000 K at $r = 0.6$ a. As a consequence, the Balmer jump is much reduced for an outer disk radius $r_{out} = 0.6$ a, and is absent for $r_{out} = 0.3$ a because of the higher temperature. The slope of the continuum flux level of an $r_{out} = 0.3$ a accretion disk is steeper (bluer) than that of an $r_{out} = 0.6$ a accretion disk, but since the smaller disk has a smaller emitting surface, its flux (for the same $\dot{M}$) is lower than that of the larger disk. As a consequence, the smaller disk requires a larger $\dot{M}$ (than the larger disk) when fitting the observed spectrum (since the disk models are scaled to the distance). When fitting the HST spectrum, the small disk models were too steep in the optical, while those with a large outer radius exhibited a small Balmer jump that was not observed. These anomalies are, however, a well-known problem in the modeling of CV WDs accreting at a high rate such as nova-like stars in high state and dwarf novae in outburst (e.g., R. A. Wade 1984, 1988; C. La Dous 1991; K. S. Long et al. 1991; A. P. Linnell et al. 2007; R. T. Hamilton et al. 2007; R. E. Puebla et al. 2007; P. Godon et al. 2017; R. Gilmozzi & P. Selvelli 2024). Many suggestions have been advanced to explain the discrepancy and address the problem, such as modifying the disk radial temperature profile (K. S. Long et al. 1994; R. E. Puebla et al. 2007; A. P. Linnell et al. 2010) or increasing the inner radius of the inner disk (A. P. Linnell et al. 2005; P. Godon et al. 2017). Some suggested irradiation of the disk (M. Kromer et al. 2007), while others suggested emission from disk winds (J. H. Matthews et al. 2015). More recently large-scale magnetic fields radially transporting angular momentum and energy have been invoked (C. J. Nixon & J. E. Pringle 2019), as well as a disk model where the energy dissipation occurs as a function of height (z) resulting in emission from optically thin regions (I. Hubeny & K. S. Long 2021). The problem is still a matter of debate and could actually be a combination of several of the scenarios suggested here together (G. Zsidi et al. 2024).

Another source of uncertainty in disk modeling has been the orbital modulation of the continuum flux level observed both in the UV and optical with a relative amplitude of 8%–9%. This has been, so far, attributed to the geometry of the system where the disk likely self-eclipses due to its higher vertical extent where it is hit by the L1 stream (J. Patterson et al. 1998, 2017).

We note that C. Knigge et al. (2022) suggest that the unusually high mass accretion rate in T Pyx could be the result of triple binary evolution. In that scenario, due to the disturbing effect of a distant companion (the tertiary), the inner binary (WD + secondary) orbit can be significantly eccentric,

triggering mass transfer close to periastron passage (e.g., J. F. Sepinsky et al. 2007, 2009, 2010). This periodic gas stripping can drive the secondary out of thermal equilibrium and intense bursts of mass accretion onto the WD can then kick-start an irradiation-induced wind-driven mass transfer phase (C. Knigge et al. 2000). C. Knigge et al. (2022) conclude that the current high-$\dot{M}$ state of T Pyx is likely associated with the high eccentricity of the (inner) binary orbit in the triple system. In that case, the light-curve variability of T Pyx might not be due only to the geometry of the rotating binary system, instead it would be affected by the periodic mass transfer/stripping near periastron (periodic increased in $\dot{M}$) and its accretion onto the WD. The nonzero eccentricity of the binary orbit is consistent with the possibility of the asynchronous rotation raised by J. Patterson et al. (2017).

Though the mass accretion rate we derived of $\sim 10^{-7}$ $M_{\odot}$ yr^{-1} cannot be firmly confirmed due to all the uncertainties cited above, it is consistent with previous estimates (e.g., J. Patterson et al. 2017). In order for our modeling to agree with M. M. Shara et al. (2018)'s accretion rate, we would have to assume a much smaller reddening and distance, which would be inconsistent with the Gaia distance and the lower limit for the reddening.

One might argue that the relatively high mass accretion rate we obtain ($> 10^{-7}$ $M_{\odot}$ yr^{-1}) must result in steady nuclear burning on the WD surface and/or affect the WD structure (inflating the radius of its outer envelop). However, the supersoft X-ray emission in T Pyx began to turn off 6 months after the outburst (L. Chomiuk et al. 2014), an indication that the nuclear burning on the WD surface stopped. Furthermore, the COS FUV spectral slope is consistent with that of an accretion disk and does not accommodate for any significant contribution from a hot WD component. If we try to fit the FUV slope with a single temperature component, it is consistent with a temperature of the order of 30–40,000 K only. This implies that the flux we observed is likely due almost entirely to the accretion disk. Interestingly enough, the optical light curve of T Pyx (attributed to the L1-inflated disk rim eclipsing the heated secondary) is very similar to the light curve of one of the prototype supersoft X-ray sources, CAL 87 (E. Meyer-Hofmeister et al. 1997), as already pointed out by J. Patterson et al. (1998).

In spite of all these uncertainties, it is uncontrovertible that the UV flux, and therefore the mass accretion rate, is now below its preoutburst level by about 40%. This large decrease in $\dot{M}$ in the ~decade after the 2011 outburst is in sharp contrast with the rather constant preoutburst UV flux from the IUE spectra. No such data were collected after the previous outburst for comparison, as the earliest IUE spectrum was obtained in 1980, 13.5 yr after the 1966 December–1967 January outburst. However, all the IUE spectra obtained through the 90s have the same continuum flux level as the 1980 IUE spectrum and show no drop in flux (except for orbital variation).

For comparison, B. E. Schaefer et al. (2013) showed that since its outburst in 1890, the mass accretion rate in T Pyx has been declining by a factor of 5.7 in 122 yr, while the UV 40% decrease in 12 yr translates into a decline by a factor of ~165 in ~120 yr, which is a factor of ~29 faster. Even in the optical, the AAVSO data show a decline of about 1 mag (V band) since its pre-2011 outburst value to present day, which is almost twice as fast as in the 1890–2011 light-curve data. This could be an indication that the self-sustained feedback loop between the WD

and secondary might is shutting off at an accelerating rate after the last outburst, in agreement with the hibernation theory.

Observations in the next 5–10 yr will be able to assess whether $\dot{M}$ continues to drop at such a high rate, or whether this is just part of a phase related to the decline from the 2011 outburst. For example, the UV flux level could reach a plateau within the next few years, based on the post-1966–67 outburst IUE data showing a constant flux level through the 80s and 90s, and assuming the behavior of T Pyx is to be the same. In that case the drop in $\dot{M}$ is much more pronounced in the decade following each outburst (and possibly due to the outburst itself). Otherwise, if the UV flux continues to drop at the same rate, mass transfer will likely completely shut off within a few hundred years and T Pyx will enter a hibernation state. Our analysis comes to further confirm that T Pyx is now in a short-lived peculiar phase of its evolution.

Acknowledgments

Software: IRAF (NOAO PC-IRAF Revision 2.12.2-EXPORT SUN; D. Tody 1993), TLUSTY (v203), SYNSPEC (v48), ROTIN (v4; I. Hubeny & T. Lanz 2017a, 2017b, 2017c), PGPLOT (v5.2), Cygwin-X (Cygwin v1.7.16), xmgrace (Grace v2), and XV (v3.10).

ORCID iDs

Patrick Godon ● https://orcid.org/0000-0002-4806-5319
Edward M. Sion ● https://orcid.org/0000-0003-4440-0551
Robert E. Williams ● https://orcid.org/0000-0002-3742-8460
Matthew J. Darnley ● https://orcid.org/0000-0003-0156-3377
Jennifer L. Sokoloski ● https://orcid.org/0000-0002-8286-8094
Stephen S. Lawrence ● https://orcid.org/0000-0002-7491-7052

References

Bode, M. F., & Evans, A. 2008, Classical Noave (2nd ed.; Cambridge: Cambridge Univ. Press)
Chomiuk, L., Nelson, T., Mukai, K., et al. 2014, ApJ, 788, 130
Darnley, M. H., Hounsell, R., Godon, P., et al. 2017, ApJ, 849, 96
De Gennaro, A., Shore, S. N., Schwartz, G. J., et al. 2014, A&A, 562, 28
Duerbeck, H. W., & Seitter, W. C. 1979, Msngr, 17, 1
Fitzpatrick, E. L., & Massa, D. 2007, ApJ, 663, 320
Gillmozzi, R., & Selvelli, P. 2007, A&A, 46, 593
Gilmozzi, R., & Selvelli, P. 2024, A&A, 681, 83
Godon, P., & Sion, E. M. 2023, ApJ, 950, 139
Godon, P., Sion, E. M., Balman, S., & Blair, W. P. 2017, ApJ, 846, 52
Godon, P., Sion, E. M., Starrfield, S., et al. 2014, ApJL, 784, L33
Godon, P., Sion, E. M., Szkody, P., & Blair, W. P. 2020, MNRAS, 494, 5244
Godon, P., Sion, E. M., Williams, R. E., & Starrfield, S. 2018, ApJ, 862, 89
Goodman, J. 1993, ApJ, 406, 596
Hack, M., Ladous, C., Jordan, S. D., et al. 1993, Monograph Series on Nonthermal Phenomena in Stellar Astmospheres (Washington, DC: NASA)
Hamilton, R. T., Urban, J. A., Sion, E. M., et al. 2007, ApJ, 667, 1139
Harrison, T. E. 2018, ApJ, 861, 102
Hillman, Y. 2021, MNRAS, 505, 3260
Hillman, Y., Shara, M. M., Prialnik, D., & Kovetz, A. 2020, NatAs, 4, 886
Hubeny, I., & Lanz, T. 2017a, arXiv:1706.01859
Hubeny, I., & Lanz, T. 2017b, arXiv:1706.01935
Hubeny, I., & Lanz, T. 2017c, arXiv:1706.01937
Hubeny, I., & Long, K. S. 2021, MNRAS, 503, 5534
Izzo, L., Pasquini, L., Aydi, E., et al. 2024, A&A, 686, 72
Knigge, C., King, A. R., & Patterson, J. 2000, A&A, 364, L75
Knigge, C., Toonen, S., & Boekholt, T. C. N. 2022, MNRAS, 514, 1895
Kramida, A., Ralchenko, Yu., Reader, J. & NIST Team 2023, NIST Atomic Spectra Database, v5.11, National Institute of Standards and Technology, https://physics.nist.gov/asd
Kromer, M., Nagel, T., & Werner, K. 2007, A&A, 475, 301
La Dous, C. 1991, A&A, 252, 100
La Dous, C. 1994, SSRv, 67, 1
Linnell, A. P., Godon, P., Hubeny, I., Sion, E. M., & Szkody, P. 2007, ApJ, 662, 1204
Linnell, A. P., Godon, P., Hubeny, I., Sion, E. M., & Szkody, P. 2010, ApJ, 719, 271
Linnell, A. P., Szkody, P., Gänsicke, B. T., et al. 2005, ApJ, 624, 923
Livio, M., & Pringle, J. E. 2011, ApJL, 740, L18
Long, K. S., Blair, W. P., Davidsen, A. F., et al. 1991, ApJL, 381, L25
Long, K. S., Wade, R. A., Blair, W. P., Davidsen, A. F., & Hubeny, I. 1994, ApJ, 426, 704
Matthews, J. H., Knigge, C., Long, K. S., Sim, S. A., & Higginbottom, N. 2015, MNRAS, 450, 3331
Meyer-Hofmeister, E., Schandl, S., & Meyer, F. 1997, A&A, 321, 245
Nixon, C. J., & Pringle, J. E. 2019, A&A, 628, A121
Paczyński, B. 1965, AcA, 15, 197
Paczyński, B. 1977, ApJ, 216, 822
Patterson, J. 1984, ApJS, 54, 443
Patterson, J., Kemp, J., Shambrook, A., et al. 1998, PASP, 110, 380
Patterson, J., Oksanen, A., Kemp, J., et al. 2017, MNRAS, 466, 581
Pringle, J. E. 1981, ARA&A, 19, 137
Puebla, R. E., Diaz, M. P., & Hubeny, I. 2007, AJ, 134, 1923
Sasseen, T. P., Hurwitz, M., Dixon, W. V., & Airieau, S. 2002, ApJ, 566, 267
Savage, B. D., & Mathis, J. S. 1979, ARA&A, 17, 73
Schaefer, B. E. 2018, MNRAS, 481, 3033
Schaefer, B. E., Landolt, A. U., Linnolt, M., et al. 2013, ApJ, 773, 55
Schaefer, B. E., Pagnotta, A., & Shara, M. 2010, ApJ, 708, 381
Schatzman, E. 1949, AnAp, 12, 281
Selvelli, P., Cassatella, A., Gilmozzi, R., & Gonzalez-Riestra, R. 2008, A&A, 492, 787
Selvelli, P., & Gilmozzi, R. 2013, A&A, 560, 49
Sembach, K. R., Howk, J. C., Savage, B. D., Shull, J. M., & Oegerle, W. R. 2001, ApJ, 561, 573
Sepinsky, J. F., Willems, B., Kalogera, V., & Rasio, F. A. 2007, ApJ, 667, 1170
Sepinsky, J. F., Willems, B., Kalogera, V., & Rasio, F. A. 2009, ApJ, 702, 1387
Sepinsky, J. F., Willems, B., Kalogera, V., & Rasio, F. A. 2010, ApJ, 724, 546
Shakura, N. I., & Sunyaev, R. A. 1973, A&A, 24, 337
Shara, M. M., Livio, M., Moffat, A. F. J., & Orio, M. 1986, ApJ, 311, 163
Shara, M. M., Prialnik, D., Hillman, Y., & Kovetz, A. 2018, ApJ, 860, 110
Shore, S. N., Augusteijn, T., Ederoclite, A., & Uthas, H. 2011, A&A, 533, L8
Sokoloski, J., Crotts, A. P. S., Lawrence, S., & Uthas, H. 2013, ApJL, 770, L33
Starrfield, S., Bose, M., Iliadis, C., et al. 2020, ApJ, 895, 70
Starrfield, S., Sparks, W. M., & Truran, J. W. 1985, ApJ, 291, 136
Starrfield, S., Truran, J. W., Sparks, W. M., & Kutter, G. S. 1972, ApJ, 176, 169
Thorstensen, J. R., Fenton, W. H., Patterson, J., et al. 2002, PASP, 114, 1117
Tody, D. 1993, in ASP Conf. Ser. 52, Astronomical Data Analysis Software and Systems II, ed. R. J. Hanisch, R. J. B. Brissenden, & J. Barnes (San Fransisco, CA: ASP), 173
Tofflemire, B. M., Orio, M., Page, K. L., et al. 2013, ApJ, 779, 22
Uthas, H., Knigge, C., & Steeghs, D. 2010, MNRAS, 409, 237
Wade, R. A. 1984, MNRAS, 208, 381
Wade, R. A. 1988, ApJ, 335, 394
Webbink, R. F., Livio, M., Truran, J. W., & Orio, M. 1987, ApJ, 314, 653
Whelan, J., & Iben, I. 1973, ApJ, 186, 1007
Yaron, O., Prialnik, D., Shara, M. M., & Kovetz, A. 2005, ApJ, 623, 398
Zsidi, G., Nixon, C. J., Naylor, T., & Pringle, J. E. 2024, MNRAS, 532, 592